ACS Partner Journal

ACCOUNTS of materials research

pubs.acs.org/amrcda

Article

This article is made available for a limited time sponsored by ACS under the ACS Free to Read License, which permits copying and redistribution of the article for non-commercial scholarly purposes.

ACS FREE TO READ LICENSE

Nanoscale Cinematography of Soft Matter System under Liquid-Phase TEM

Zihao Ou, Chang Liu, Lehan Yao, and Qian Chen*

Cite This: https://dx.doi.org/10.1021/accountsmr.0c00013

Read Online

ACCESS | Metrics & More | Article Recommendations

CONSPECTUS: One emergent theme in "soft matter" is to understand and manipulate the self-organization of synthetic materials and biological entities in space and time at the underexplored nanoscale. Encoded at this length scale can be a diversity of spatiotemporally fluctuating dynamics that are critical to function, from phase transition of nanoparticle self-assemblies as reconfigurable devices and morphology development of polymer membranes as separation layers for wastewater reclamation to the transformation of membrane proteins as the gatekeeper for mass and information flow in living cells. Extensive research efforts have thus been focused on resolving and understanding such dynamics that typically occur in a liquid medium. The proliferation of methods such as liquid-phase atomic force microscopy, cryogenic electron microscopy, and super-resolution optical microscopy has greatly expanded our knowledge in the structure or dynamics of soft matter at the nanoscale. However, these techniques do not offer direct real-space, real-time imaging of the structural and functional dynamics in a native liquid environment with nanometer resolution. This lack of experimental dataset also renders predictive modeling or computation difficult. As a result, how nanoscale morphology and interaction of the constituents affect the self-organization pathways or broadly collective structural evolution, such as interconversion among metastable states, as well as the involved energy measures remains poorly understood.

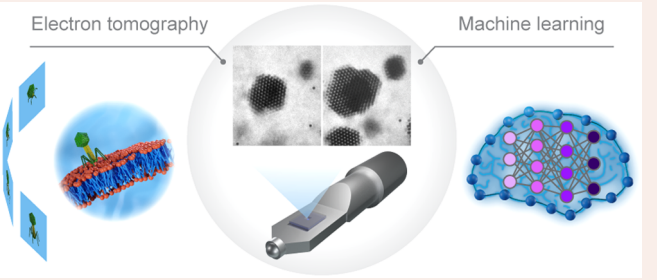

In this Account, we present our recent efforts in adapting and using a nanoscopic cinematography method relatively new to the soft matter community, liquid-phase transmission electron microscopy (TEM), to study the self-organization pathways of nanoscale colloidal matter. Liquid-phase TEM has opened a new avenue to investigate materials chemistry questions, such as electrochemistry and catalysis, nanomaterial diffusion and growth, and nucleation of minerals and atomic crystals. Applying it to soft matter systems involves tackling complications, including the electron beam's modification of nanoscale colloidal interaction and the substrate effect present in the liquid chamber, for both of which we highlight achievements of control. In addition, we discuss a series of first-time imaging of self-organization pathways of nanoparticle systems, accessible only by liquid-phase TEM. At low nanoparticle concentrations, chaining of nanoparticles occurs following quantitatively the kinetic laws of polymerization. This analogy originated from local collision and pairwise interaction, which can be directly mapped from trajectory sampling. At high nanoparticle concentrations, collective phase behaviors such as crystallization and coalescence are observed with single-particle resolution, allowing for the charting of phase coordinates and thermodynamic quantities based on statistical mechanics principles. We also discuss the general applicability of these methods. Lastly, toward taking live videos of organic soft matter at the nanoscale, we highlight recent instrumental developments, including machine learning based liquid-phase TEM video analysis to account for low signal-to-noise ratio data sets and low-dose electron tomography to resolve three-dimensional morphologies. We foresee that the examples, techniques, and understandings pinpoint the beginning of a paradigm shift in soft matter studies, where knowledge at the nanoscale can be derived from direct "seeing".

1. INTRODUCTION

de Gennes first used the term "soft matter" in his 1991 Nobel lecture to describe broadly systems that are complex and flexible,[1] constructed often from tiny constituents that can be agitated by thermal fluctuations in their suspended liquid media, with *dynamics* as their common middle name. Here *dynamics* covers phenomena from structural, phase, and functional changes of the materials as a whole (such as in a colloidal suspension) to the motion and transformation of

Received: July 15, 2020
Revised: September 29, 2020

Downloaded via UNIV ILLINOIS URBANA-CHAMPAIGN on October 9, 2020 at 18:24:29 (UTC).
See https://pubs.acs.org/sharingguidelines for options on how to legitimately share published articles.

ACS Publications

© XXXX Accounts of Materials Research. Co-published by ShanghaiTech University and American Chemical Society. All rights reserved.

single constituents. Since then, multiple fields of research have been developed as supported by different underpinning characterization methods. On the end of large yet thermally agitable constituents, colloidal physics has established interaction models to describe myriad phase transition dynamics (e.g., nucleation, melting, solid-to-solid transition), based on the direct imaging of micrometer-sized colloids at the single particle level by optical microscopy (OM).[2] As the size of the constituents decreases, biophysics relies on various versions of super-resolution OM techniques to bring the diffraction-limited hundreds of nanometers resolution to tens of nanometers resolution for biomolecular systems. Yet this resolution is only for locating the centroids of individual fluorophores.[3] Further understanding of details, such as the structure, function, and rotational dynamics of single biomolecules, still relies heavily on molecular dynamics simulation. For similarly sized synthetic polymers as the constituents, polymer physics builds mostly on mean-field theories and ensemble experimental measurements (rheology, X-ray scattering, diffraction, etc.) instead of direct imaging to predict and verify scaling laws relating properties of a polymer or polymer suspension to the basic structural attribute of degree of polymerization.[4] In these diverse fields of research, taking real-space, real-time videos of dynamics, which we refer to as the art of cinematography, is powerful in providing insights on motions, interactions, and phase changes at the single constituent level. However, such cinematography has been mostly using OM and significantly less explored in transmission electron microscopy (TEM), although TEM offers the unparalleled capability of resolving morphology at the nanometer and even atomic spatial resolution. The challenge has been well-known: the beam of imaging electrons transmitted through samples in TEM needs to be kept at high vacuum[5] and is incompatible with suspension forms of soft matter.

In this Account, we discuss our research on using a recent adaptation of TEM, in situ liquid-phase TEM, to gain insights into soft matter at the underexplored nanoscale. Compared with the micrometer-sized constituents where cinematography is mature and so are the understandings of their phase behaviors, each system consisting of nanosized constituents is phenomenologically different in its own way. On one hand, nanosized constituents are vastly different in composition, structure, and function.[6] Nature routinely achieves functions such as molecular recognition, directed transport, feedback regulation, and selective catalysis via structural fluctuations of biomolecules. Here structural variation as small as pore opening and closing can cause switching of healthy or diseased states of biomolecules differentiated by energy differences as small as a few k_BT.[4] Though not built from precise sequences of amino acids or nucleic acids, abiological nanosized constituents also exhibit hard-to-unify behaviors. For example, iron oxide minerals nucleate from nanosized cages of solvated ions,[7] while coral skeletons grow from solid nanoparticle forms of amorphous calcium carbonate.[8] On the other hand, despite extensive experimental observations, explanations of the kinetic pathways and associated energetics of the self-organization, determining intermediates, polymorphs, and their interconversions, are still in their infancy due to multiple challenges.[9] Interactions between nanosized constituents governing all these transitions are considerably more complex to model and predict than those between micrometer-sized colloids. Nanosized constituents can have sizes comparable to local structures of solvents, ions, and ligand molecules, which are smeared out for micrometer-sized colloids due to a huge separation in dimensions but need to be thoroughly considered in modeling nanosized constituents.[10] In this case, the lack of direct experimental observation on the motion, interaction, and kinetic pathways due to the limited implementation of cinematography makes it difficult to construct and validate models. The disparity between the wide relevance of self-organization of nanosized constituents and the limited understanding suggests great potential for in situ liquid-phase TEM to provide experimental data sets and understandings that are otherwise inaccessible.

We will focus on our group's efforts in adapting the nanoscopic cinematography to study the rules of self-organization of nanoscale colloidal matter (i.e., nanoparticles) (Figure 1), the topical relevance of which is different from other reviews on the technical development,[5] chemical reaction dynamics,[11] and cellular imaging[12,13] of liquid-phase TEM. Studying self-organization of nanoparticles requires meticulous "taming" of the beam-intensive and geometrically confined (liquid thickness less than ~1 μm) liquid environ-

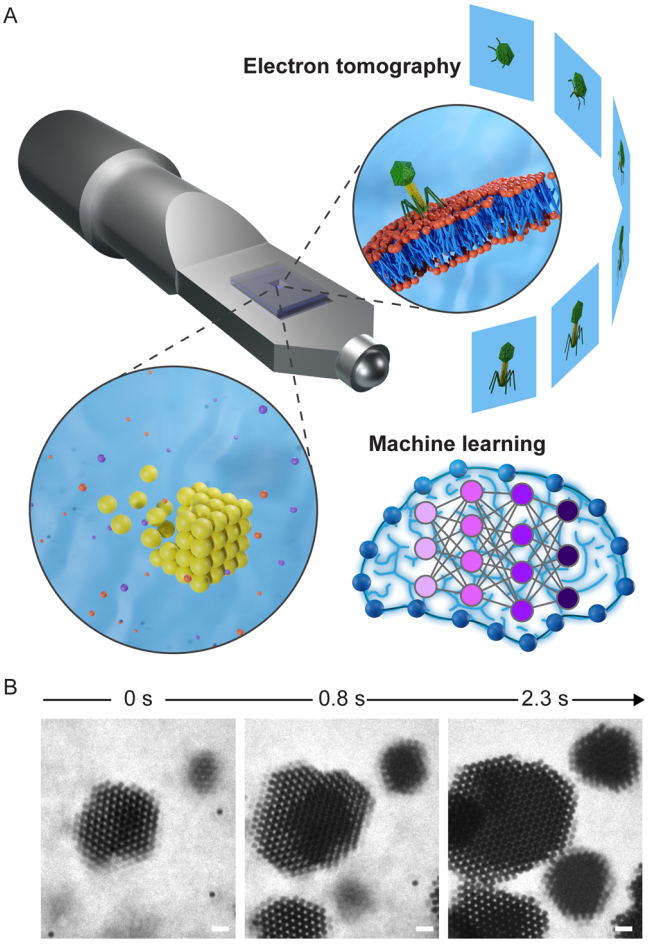

Figure 1. Liquid-phase TEM based cinematography on soft matter at the nanoscale. (A) Schematic of liquid-phase TEM with typical soft matter systems (bacteriophage on a lipid membrane, top; inorganic nanoparticles, bottom) encapsulated, which can be coupled with electron tomography and machine learning. (B) Representative dynamic features captured by liquid-phase TEM such as crystallization of nanoparticle superlattices. Reproduced with permission from ref 17. Copyright 2019 Springer Nature. Scale bars = 100 nm.

https://dx.doi.org/10.1021/accountsmr.0c00013
Acc. Mater. Res. XXXX, XXX, XXX−XXX

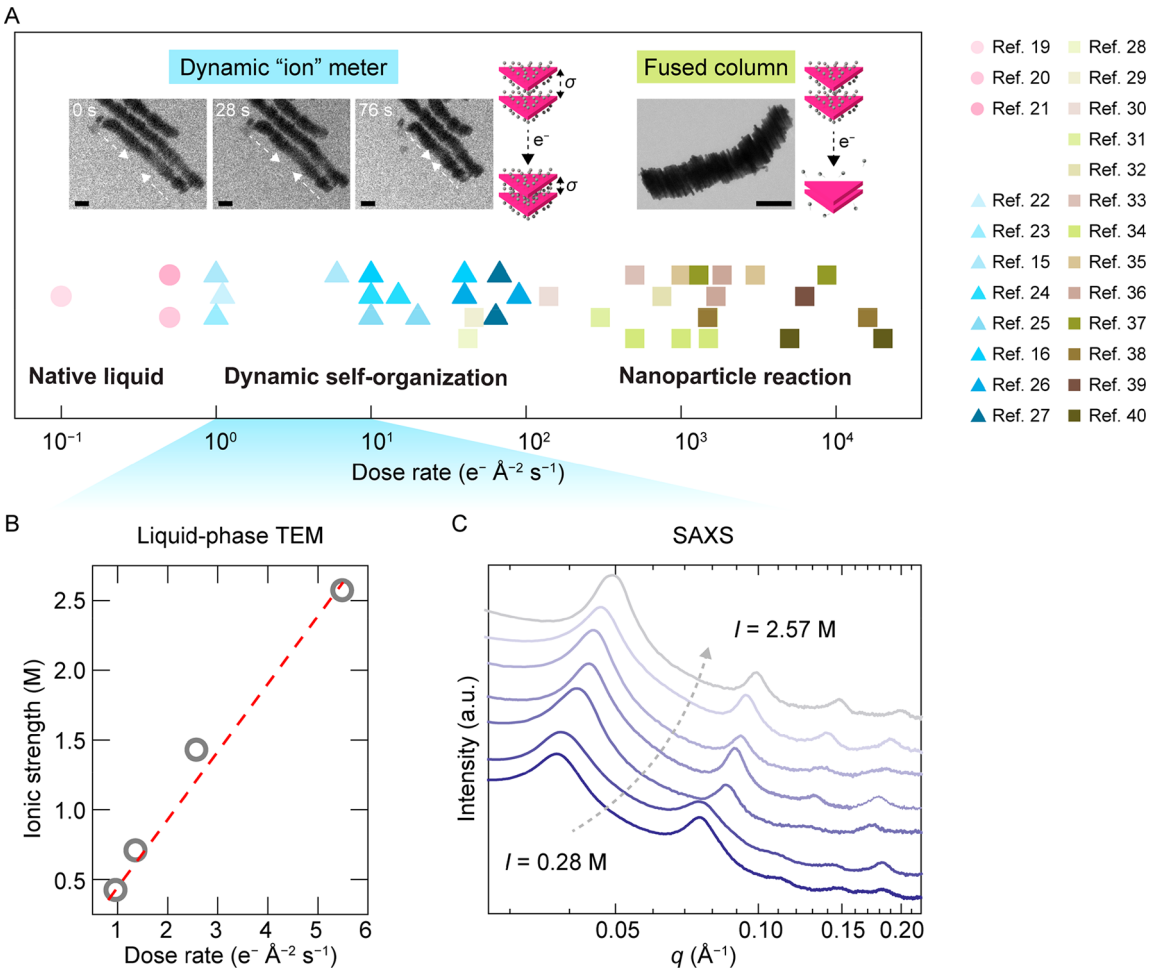

Figure 2. Dose rate diagram. (A) Scatter plot of electron beam dose rates used in previous liquid-phase TEM literature and the corresponding beam effects. Inset, TEM images show the behaviors of the ion meter in the "dynamic self-organization" and "nanoparticle reaction" regimes. (B) Effective ionic strength (I) at different dose rates with an initial I = 0.42 M (0.15 M, pH = 8, phosphate buffer solution). The dotted line is a guide to the eye. (C) SAXS measurements of the ion meter at I = 0.28, 0.42, 0.57, 0.71, 0.99, 1.43, and 2.57 M (bottom to top). Reproduced with permission from ref 15. Copyright 2016 American Chemical Society. Scale bars = 100 nm.

ment specific to liquid-phase TEM (section 2). Nanoparticles are used as structural and functional analogues of elements in the periodic table and can assemble into exotic superstructures of collective optical, magnetic, mechanical, and electronic properties.[6] They serve as our high TEM contrasting and beam tolerating model systems to study, with systematically varied structural attributes (e.g., size, shape, ligand chemistry). This variability provides a playground for us to elicit generic concepts and rules of self-organization pathways at the nanoscale from liquid-phase TEM observations (section 3). The imaging and analysis protocols that we have established and are developing can be extended to organic soft matter (section 4), with future direction and opportunities discussed in section 5.

2. "TAMING" LIQUID-PHASE TEM FOR IMAGING SELF-ORGANIZATION OF SOFT MATTER

Soft matter features the ability to respond to environmental fluctuation.[1] It is thus of key significance to understand and control its surrounding liquids, which can be altered during liquid-phase TEM imaging. In this section, we discuss two aspects of liquid-phase TEM that we tame to observe credible in situ dynamics consistent with the ensemble behaviors probed outside TEM. One aspect comes from the electron beam. Extensive reviews have discussed the electron-induced radiolysis of solvents.[5,12−14] We focus on our work that calibrates beam effects explicitly on nanoscale interactions. The other is on the substrate of a liquid TEM chamber sandwiching the sample. The existence of substrates is important to consider, because a decent portion of the liquid sample is in physical contact with the substrate due to the ultrathin liquid volume encapsulated in the chamber. We find these two aspects most relevant to studying the self-organization pathways of nanoscale soft matter, while other effects such as heating, convection flow, and charging are often negligible at our imaging conditions.[14−18]

2.1. "Dose Rate Diagram" to Calibrate Nanoscale Interparticle Interactions

Our first independent work measures electron beam effects on nanoscale interactions by correlating liquid-phase TEM with small-angle X-ray scattering (SAXS), the latter being a prevalent noninvasive characterization tool to elucidate the ensemble structures of nanoscale assemblies.[15] Specifically, we use a one-dimensional (1D) superlattice assembled from gold triangular nanoprisms as an "ion" meter to monitor beam-induced ion generation via radiolysis of water. This superlattice

https://dx.doi.org/10.1021/accountsmr.0c00013
Acc. Mater. Res. XXXX, XXX, XXX−XXX

has an equilibrium lattice constant σ, measurable under liquid-phase TEM as the nearest neighboring prism-to-prism distance, that monotonically depends on the solution ionic strength, namely, valency-weighted concentration of ions. Using this ion meter, we measure, on one hand, the curve relating σ to electron dose rates (number of electrons shining per unit area per unit time) and, on the other hand, the curve relating σ to the ionic strength using SAXS.

In doing so, we chart a dose rate diagram (Figure 2A), which shows three regimes, matching with our literature survey on 24 papers with documented dose rates. At low electron dose rates (<1 $e^- Å^{-2} s^{-1}$), no structural alteration of the superlattice is observed under liquid-phase TEM, suggesting the absence or suppression of radiolysis reactions.[15] This regime can be used for imaging systems with low tolerance to radiolysis products, such as biomolecules, polymers, and electrochemical processes.[5,13,19−21] At intermediate electron dose rates (<100 $e^- Å^{-2} s^{-1}$), radiolysis products have low concentration and do not react with metal nanoparticles to alter their shape.[15,16,22−27] Nevertheless, the ions generated impact the electrostatic interaction, as shown in the one-to-one plot charting electron dose rates with the effective ionic strength (Figure 2B,C).[15] We use this regime to study self-organization pathways (section 3) where the electron beam serves as a quantitative and predictable handle to change the nanoscale colloidal interactions in situ. At even higher electron dose rates (>100 $e^- Å^{-2} s^{-1}$), the ligands capping nanoparticles can be stripped off or decomposed by the electron beam.[15] This regime has been used extensively to study the shape transformation of inorganic nanoparticles, such as nucleation, coalescence, and growth,[28−40] but can be detrimental to studying self-organization pathways where the constituents shall not experience beam-induced alteration.

Besides electron dose rates, total dose is relevant to biomolecules and polymers. Continuous flow of solvent can minimize the accumulation of radiolysis species. Different types of solutions (e.g., buffer, radical scavenger, D_2O) can be used to further minimize radiolysis during liquid-phase TEM imaging, to mimic practical experiments outside TEM.[13,14] The radiolysis products generated during imaging are shown to reach a steady concentration within seconds,[5,15] allowing for in situ modulation of interparticle interactions upon temporal changes in dose rates, to trigger and study structural reconfiguration upon changes in surrounding chemical species.

2.2. Modulating Diffusional Dynamics by Substrate−Nanoparticle Interaction

The diffusional dynamics of nanoparticles or broadly nanosized constituents determine how fast they approach, interact, and sample the free energy landscape, thereby imposing impacts on the self-organization pathways. In using liquid-phase TEM, while substrate effects have been discussed in various scenarios such as heterogeneous nucleation mediated by chemical heterogeneity of the SiN_x chip,[41] we find in the "dynamic self-organization" regime of dose rates (Figure 2A), substrates contribute predominantly by modulating the diffusional dynamics of nanoparticles.

Most commercial SiN_x substrates, upon beam illumination, are positively charged as balanced by input and output currents[14] and thus exhibit electrostatic attraction to negatively charged nanoparticles (Figure 3A). In the example of gold nanoarrows (GNAs),[42] when dispersed in deionized water, the negatively charged GNAs can rapidly adsorb onto the substrate

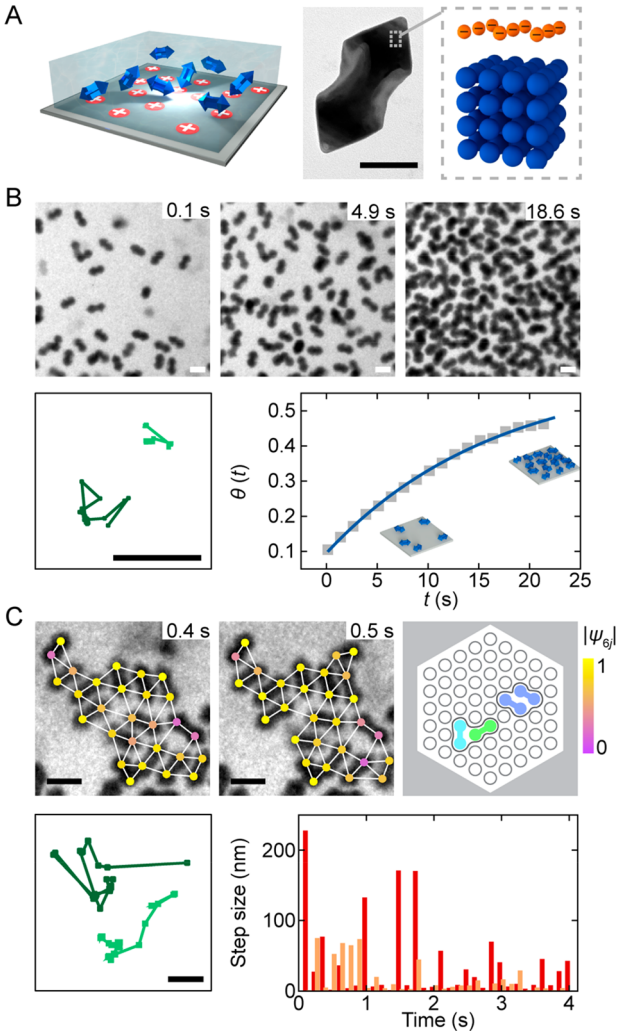

Figure 3. Modulation of nanoparticle diffusional dynamics by substrate−nanoparticle interaction. (A) Schematics and TEM image of GNAs dispersed in SiN_x liquid chamber. (B) (top) Time-lapse TEM images showing GNA adsorption onto the SiN_x chip during imaging at I = 4.9 μM. (bottom) Trajectories of two typical GNAs (left) and graph of the occupied areal fraction θ versus time t fitted by the kinetic Langmuir model (blue line, right). (C) (top) Time-lapse TEM images and schematics showing assembly of GNAs into DC-like structures at I = 6.4 mM. (bottom) Trajectories of two typical GNAs (left) and the step sizes at a fixed time interval of 0.1 s (right). Scale bars: panel A, 50 nm; panels B and C, 100 nm. Reproduced with permission from ref 42. Copyright 2020 American Chemical Society.

due to electrostatic attraction, following Langmuir adsorption and exhibiting no self-organization (Figure 3B). In contrast, when the substrate−nanoparticle attraction weakens, nanoparticles diffuse quickly and sample the free energy landscape efficiently, which is essential for collective behaviors to emerge. For example, in the same GNA system, increased ionic strength screens the electrostatic substrate−nanoparticle attraction, leading to the assembly of GNAs into degenerate crystal (DC)-like structures (Figure 3C) and atom-mimicking coalescence (section 3.4). Similarly, in the system of negatively charged gold nanoprisms,[17] fast diffusion is retrieved at high ionic strength, which facilitates our first-time observation of the nucleation pathways of superlattices (section 3.3). The impact of substrate−nanoparticle interaction on the diffusional dynamics of nanoparticles can be system-specific[14] (e.g.,

https://dx.doi.org/10.1021/accountsmr.0c00013
Acc. Mater. Res. XXXX, XXX, XXX−XXX

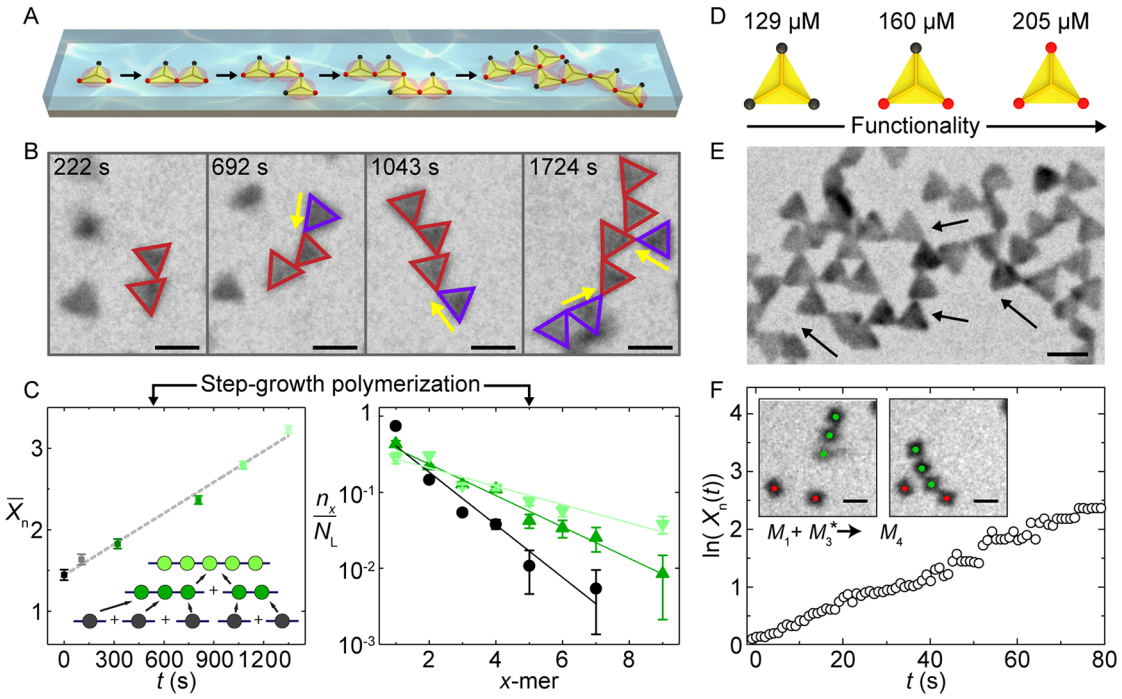

Figure 4. "Polymerization" kinetics at the low nanoparticle concentration limit. (A, B) Schematics (A) and time-lapse TEM images (B) showing bifunctional gold prisms self-organizing into linear chains. (C) (left) Graph showing $\overline{X}_n$ relating linearly to assembly time t. (right) Semilog plot showing the fraction of x-mers (n_x/N_L) at different t following Flory–Schulz distribution. (D) Schematics illustrating the increase in I leading to increased functionality of prisms (red denoting connectable tips). (E) TEM snapshot of the cyclic assemblies. (F) Plot of $\ln(\overline{X}_n(t))$ versus t and TEM images (inset) showing gold nanocubes self-organizing into chains following a first-order reaction. Scale bars = 100 nm. Panels A–E reproduced with permission from ref 16. Copyright 2017 Springer Nature. (F) Reproduced with permission from ref 43. Copyright 2020 American Chemical Society.

superdiffusive, Lévy flight, self-propulsion) and can be modulated by the shape, size, and composition of nanoparticles to study equilibrium and out-of-equilibrium phase behaviors.

3. RULES OF SELF-ORGANIZATION PATHWAYS FOR NANOSCALE CONSTITUENTS

Abundant superstructures such as quasicrystals and hierarchical heterostructures self-organize from a huge diversity of synthetic nanoparticles thanks to materials chemists' decades of efforts.[6] The self-organization mechanism of these superstructures is often explained case-by-case, considering the synthetic attributes of nanoparticles, by global free energy minimum principles such as entropy-driven densest packing, Wulff construction, and geometric frustration.[6,18] Understanding the kinetic pathways along which superstructures are formed out of random Brownian motions of individual nanoparticles are what we contribute here. We discuss below from the low particle concentration limit where the interacting events are local between a pair of nanoparticles (sections 3.1 and 3.2) to the high particle concentration limit where collective interactions work to show phase transitions (sections 3.3 and 3.4).

3.1. "Polymerization" Kinetics Based on Local Interaction Events at the Low Nanoparticle Concentration Limit

We find in our experiments that the self-organization dynamics of nanoparticles can follow local interaction events where pairwise interaction alone can describe the pathways, a scenario that can be robustly achieved at the low nanoparticle concentration limit.[16,43] In this regime, our work on both gold triangular prisms[16] and nanocubes[43] shows that the self-organization pathways unify with the kinetic growth laws of polymers, where molecular monomers react and link into products of different topologies. If we see nanoparticles as colloidal monomers and an assembly event of two nanoparticles as a linking reaction, the self-organization can be interpreted as occurring through elementary steps involving only local reactions of identical reaction rate constants. This analogy to polymerization originates from the local nature of polymerization reactions where polymers grow with a reaction rate constant independent of the polymer molecular weight, exactly the case for nanoparticle interactions at the low nanoparticle concentration limit.[16] In contrast, if many-body effects of the system matter, the self-organization pathways no longer follow polymerization kinetics and instead generate complex superstructures such as the hierarchical lattices in section 3.3 and coalescing clusters in section 3.4.

The spontaneous chaining of gold triangular prisms into "polymers" shows complete conceptual and quantitative agreement with molecular polymerization (Figure 4), in aspects from functionality (number of linking sites per particle) and step-growth polymerization based growth laws to bonding motifs prescribed by interparticle interactions.[16] First, analogous to monomer functionality in polymer engineering, the bonding capability of individual prisms was shown to increase from bifunctional to trifunctional as we weaken the interprism electrostatic repulsion, leading to changes in the assembly topology from 1D chains (Figure 4A,B) to 2D cyclic networks (Figure 4D,E). Second, the temporal evolution of number-averaged degree of polymerization ($\overline{X}_n$) for the bifunctional prisms follows step-growth polymerization (Figure 4C), suggesting a one-to-one control over the size of the superstructures by assembly time. The third aspect of bonding

https://dx.doi.org/10.1021/accountsmr.0c00013
Acc. Mater. Res. XXXX, XXX, XXX−XXX

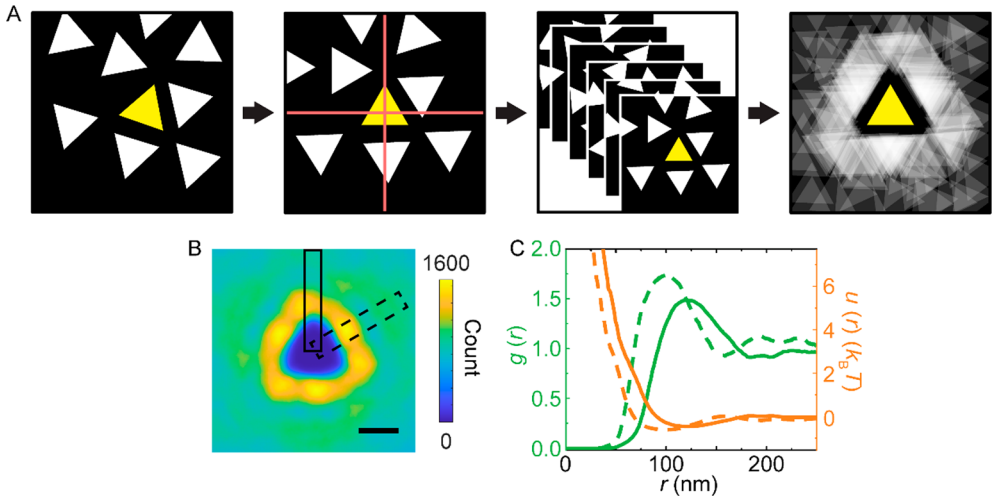

Figure 5. Mapping the effective pairwise interactions of nanoparticles. (A) Schematic showing the workflow to generate the 2D distribution map (B) with accumulated statistics from a pair of prisms where one of them is centered (yellow) and the other is overlaid to contribute to distribution counts. (C) $g(r)$ and interaction curves derived from panel B along the prism side (dashed) and prism tip (solid). Scale bar = 100 nm. Reproduced with permission from ref 43. Copyright 2020 American Chemical Society.

motifs requires consideration of nanoscale morphology detail. Flat or round tipped prisms favor a sawtooth or bowtie motif, respectively.[16]

Notably, we find that substrate−nanoparticle interaction (section 2.1) regulates the colloidal polymerization. The prisms experience a substrate−nanoparticle attraction that constrains them from moving freely in the z direction but still allows them to diffuse laterally to follow diffusion-controlled second-order step-growth polymerization.[16] In our other work on gold concave nanocubes, the substrate−nanoparticle attraction is stronger.[43] The nanocubes stay adsorbed on the substrate for 98% of the time. The linking events only occur for the occasionally desorbed nanoparticles and thus are rated limited by the desorption of the concave nanocubes, leading to first-order growth kinetics (Figure 4F). This kinetic model applies to cases where nanoparticle adsorption on a substrate is involved in self-organization, such as solvent-evaporation driven self-assembly. This ability to quantitatively understand the kinetic laws during self-organization can help control the kinetic pathways to make superstructures with desired size, dispersity, and topology at high yield.

3.2. Mapping the Effective Pairwise Interactions

At the low particle concentration limit, the bonding motifs are dictated by pairwise interactions, which can be mapped using liquid-phase TEM.[43−45] These methods are applicable to nanoparticles exhibiting anisotropic shapes, structural fluctuation, or chemical heterogeneity. We use the Boltzmann principle,[43] that is, the most sampled relative configuration in an interacting nanoparticle pair corresponds to the lowest free energy states. At steady state, the radial distribution function of nanoparticles ($g(r)$) relates to the pairwise interaction $u(r)$ through $g(r) = \exp(-u(r)/(k_BT))$, where k_B is the Boltzmann constant and T is temperature.[44] In our work on gold prisms, aided by machine learning based segmentation to recognize particle contours, we map the pairwise interaction energy landscape (Figure 5).[43] The statistics accumulated from ∼300 000 instantaneous prism pairs render an anisotropic 2D distribution map (Figure 5B), from which we extract two different forms of pairwise interactions along the tip and the side directions of prisms (Figure 5C). The potential valley along the prism side corresponds to a side-by-side motif, consistent with the densest packing structure proposed in simulations. The valley along the prism tip corresponds to a tip-to-tip motif as shown in Figure 4A, showcasing the method's potency to recognize anisotropic interaction energy landscapes.

In this and other examples[44,45] using this principle, the 2D distribution maps are plotted based on the statistics from many particles in a liquid-phase TEM video. The statistics can also be achieved by overlaying sustained trajectories of one particular pair of particles, which can be useful when the nanosized constituents structurally fluctuate over time (such as biomolecules) or are polydisperse (such as nanoplastics). The extracted pairwise interaction energy landscape can predict the bonding motifs, toward establishing a library of interaction forms at the nanoscale for modeling efforts.

3.3. Collective Phase Transition Pathways at High Nanoparticle Concentration

At high nanoparticle concentration, the nanoparticles exhibit collective phase behaviors that cannot be simply understood as addition of dynamic events at the pairwise level.[2] Instead, phase transitions involve spatiotemporal fluctuation and heterogeneity on the *cluster* level, a few or more particles locally bonded with extended network, even when each particle is identical in their own structural attributes. For example, nucleation as the first step of crystallization involves the emergence of crystallite embryos from disordered regions due to a local density fluctuation.[9] While historically micrometer-sized colloids have served as the model system to unravel phase transition pathways,[2] extrapolation into the nanoscale is difficult because the fundamental interactions of the constituents are not scalable.[4] Utilizing liquid-phase TEM, we marry the toolkits established for micrometer-sized colloids, mostly based on statistical mechanics, with the previously inaccessible data set of TEM videos of collective phase transitions resolved at the single nanoparticle level.[17] In doing so, we can measure collective properties such as the frequency histogram of phase coordinates and kinetic pathways sampling temporary traps and multiple free energy barriers.

https://dx.doi.org/10.1021/accountsmr.0c00013
Acc. Mater. Res. XXXX, XXX, XXX−XXX

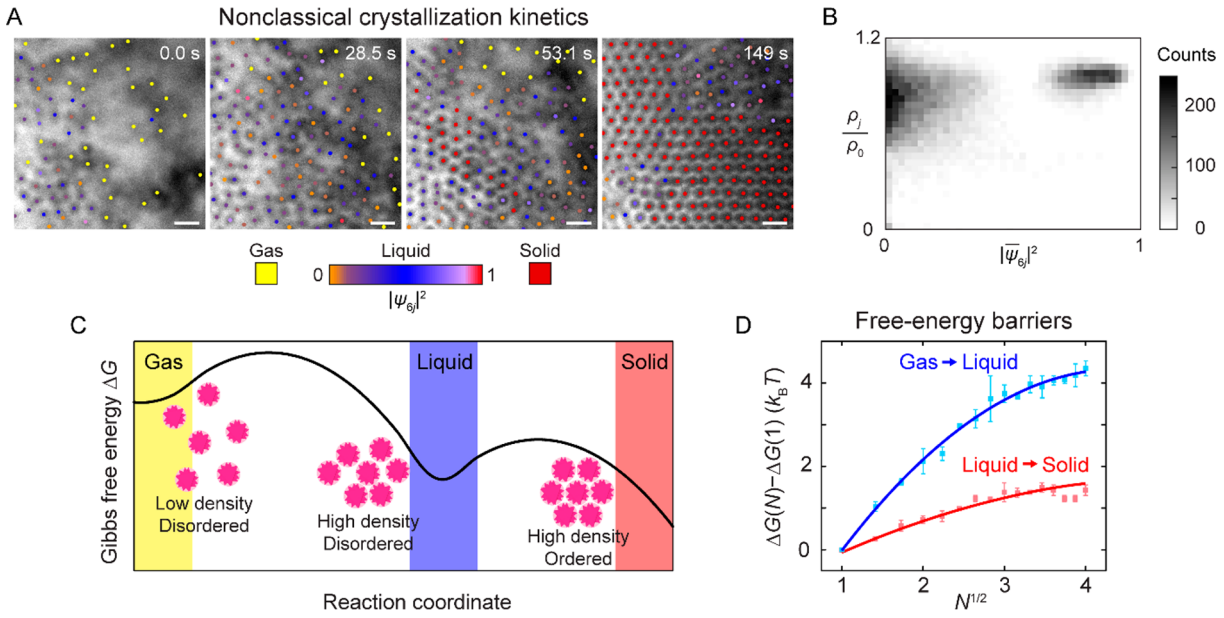

Figure 6. Nonclassical crystallization in nanoparticle superlattice. (A, C) Time-lapse TEM images (A) and schematics (C) showing the nonclassical crystallization process of gold prisms. (B) Experimentally measured 2D phase coordinates ($|\overline{\psi}_{6j}|^2$, ρ_j) during crystallization. (D) Free-energy barriers for the gas−liquid (blue) and liquid−solid (red) transitions measured based on the domain distributions. Solid lines are parabolic fittings, from which surface tensions are derived. Scale bars = 200 nm. Reproduced with permission from ref 17. Copyright 2019 Springer Nature.

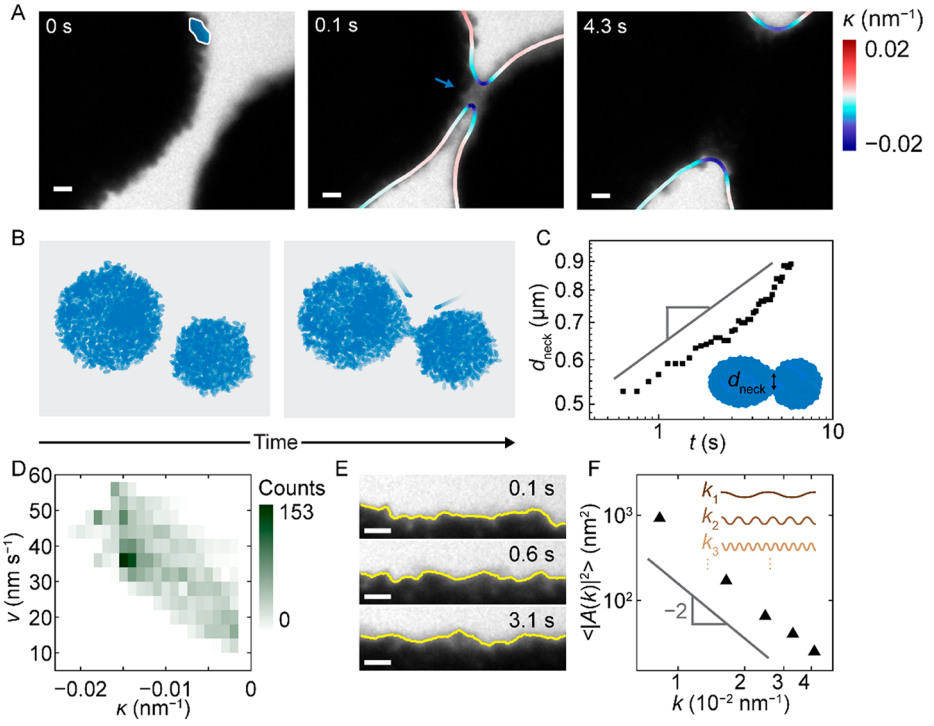

Figure 7. "Atom" mimicry of nanoparticles. (A, B) Time-lapse liquid-phase TEM images (A) and schematics (B) showing the coalescence of two GNA clusters. (C) Evolution of d_{neck} with t indicating surface diffusion. (D) Local curvature (κ)−growth rate (v) histogram showing the curvature-dependent flattening to minimize surface energy. (E) Time-lapse liquid-phase TEM images showing the fluctuating surface. (F) Dependences of $\langle|A(k)|^2\rangle$ on k on a log−log scale. Scale bars = 100 nm. Panels A and C−F reproduced with permission from ref 42. Copyright 2020 American Chemical Society.

In our first proof-of-demonstration studying pathways of nanoparticles crystallizing into superlattices,[17] we map a nonclassical crystallization with a dense amorphous structure as the intermediate, a phenomenon observed in proteins and biominerals[9] but elucidated in nanoparticle systems for the first time. We use gold triangular prisms and screen the substrate−nanoparticle interaction so that the prisms move freely in the solution to construct a 3D superlattice. The nanoparticle concentration is high for crystallization to spontaneously occur. We note three features in the crystallization pathway. First, the prisms recognize their shape anisotropy and stack first face-to-face into columns. The columns move as a whole and interact

https://dx.doi.org/10.1021/accountsmr.0c00013
Acc. Mater. Res. XXXX, XXX, XXX−XXX

to form into a hierarchical superlattice (Figure 6). Second, a large-sized crystal could only be formed due to the fast motions of the columns, which correct misalignment or mispositioning. Third, crystallization occurs with an amorphous prenucleation precursor. Liquid-phase TEM records the evolution in local structural order (characterized by the modulus squared 6-fold bond orientation order $|\psi_{6j}|^2$) and local density (ρ_j) of each column during crystallization. Clearly, we observe that a dense amorphous, that is, "liquid", phase first grows, within which the ordered "solid" phase then nucleates and expands (Figure 6A). Further charting of the 2D order−density phase coordinate validates that the "liquid" domain is indeed a metastable precursor showing as a high-probability region, characteristic of a two-step crystallization process (Figure 6B).

Furthermore, such direct imaging of phase transitions at the single constituent level allows for measurement of energetic parameters such as surface tensions of the interfaces and associated free-energy barrier.[17] In this system, surface tension characterizes the difference in the Gibbs free energy (ΔG) of the nanoparticles dispersed in suspension and those residing within the superlattice. Take the first step of liquid phase formed from dispersed "gas" phase as an example (Figure 6C). The free-energy barrier can be measured from domain size distribution using $\Delta G(N) - \Delta G(1) = -k_B T \ln(n^L(N)/n^L(1))$, where $n^L(N)$ is the count of liquid domains of size N (Figure 6D). Gas−liquid surface tension is thus calculated to be $(1.0 \pm 0.1)k_B T$ per column diameter. From the mapped Gibbs free-energy, energy barrier for this first step of crystallization is $4.3k_B T$, high but still possible for thermal fluctuation to overcome.

This work opens avenues to other phase transitions of nanosized constituents, from melting, sublimation, and molecular aggregation (e.g., scale deposition, asphaltene aggregation, biofouling), to protein folding.[2,4,5,9] This method of statistically elucidating the intermediate from a 2D phase coordinate can be applied to other systems of complex energy landscape, where the coordinates can be local crystal orientation, Lindemann parameter, and chirality index.[2,6] The measured parameters during the phase transition can serve as inputs or validations for simulations to guide minimal modeling of the kinetic pathways of self-organization at the nanoscale, and to identify key players such as the nanoscale interaction, transient intermediates, and mass transport properties.

3.4. The "Atom" Mimicry of Nanoparticles in Coalescence and Capillary Waves

The nonclassical crystallization pathway discussed in section 3.3 has similarities to those in micrometer-sized colloidal systems and scale-free simulations,[2,17] rather than representing aspects specific to the nanoscale, likely because the building blocks of that superlattice are bulky columns (hundreds of nanometers in size). In our recent work where the individual nanoparticles (GNAs here) are the building blocks,[42] they exhibit atom-like kinetics uniquely attributed to their orders of magnitude faster diffusion than that of micrometer-sized colloids. As shown in Figure 7A,B, upon triggering of self-organization, the GNAs pack into clusters, which diffuse and coalesce upon contact with a neck formed. We track the evolution of the neck width (d_{neck}), namely, the distance between the neck apexes, over time t, which exhibits a power law of $d_{neck} \sim t^{0.24}$ (Figure 7C). This power law agrees with a surface diffusion mechanism for the coalescence ($d_{neck} \sim t^{0.16}$) as predicted by the classical continuum theory accounting for the mass transportation during this process.[33]

The application of capillary wave theory (CWT) to the experimental movies allows us to discern free energy minimization by reducing surface area as the driving force for coalescence in the GNAs (Figure 7D), similar to that in atomic systems.[42] Quantitatively, the surface energy gain during coalescence is measured based on CWT, a first time implementation for interfacial fluctuations at the nanoscale on the single particle level. CWT describes how the fluctuation of a surface is defined by a balance of thermal fluctuation (roughening) and surface energy (smoothing).[18] It has been successfully applied to simulations of atomic interfaces (e.g., Ni, Ag) and experiments of micrometer-sized colloids.[18] In the GNA system, we validate the applicability of CWT to the fluctuating surface profile (Figure 7E) by decomposing its height function into a series of sinusoidal waves of wave vector k.[42] The squared time-averaged Fourier coefficient $\langle |A(k)|^2 \rangle$ fits with $k^{-2.2}$ (Figure 7F), consistent with the prediction of CWT ($\langle |A(k)|^2 \rangle \sim k^{-2}$). Upon this application, the surface energy is calculated as $(1.26 \pm 0.02) \times 10^{-13}$ J m^{-1} for this system, corresponding to a surface energy gain of $3.2k_B T$ based on the initial neck width d_{neck} (104 nm), sufficient for coalescence to happen.

This observation of atom-mimicking self-organization behaviors in this one GNA system can inspire us to study further the general applicability of this analogy. It also suggests that the synthesis toolkits of atomic crystals (e.g., seeded growth to break symmetry, single crystal growth by oriented attachment) can serve as principles to encode structure and dynamics in nanoscale self-organization.

4. TOWARD ORGANIC SOFT MATTER

Unlike inorganic nanoparticles, the structure and shape of organic soft matter, such as polymers and proteins, can be redefined by the solvent environment. For example, the function-determining 3D structures of proteins, the central dogma of structural biology, are sampled over a highly corrugated potential energy surface, encoded by solvent-mediated interactions of functional groups (e.g., hydrophobic pockets, patchy surface charges).[4] Real-space nanoscopic imaging is thus more urgently needed. However, application of liquid-phase TEM to organic soft matter encounters new challenges. Organic soft matter can have low TEM contrast due to low atomic weight composition (C, N, S, etc.), exhibiting low signal-to-noise ratio (SNR) and high beam sensitivity.[12] Moreover, they have complex 3D shapes, which are insufficiently resolved or analyzed by conventional projection-only liquid-phase TEM configuration. Below we discuss two recent efforts toward addressing these challenges.

4.1. Machine Learning for Low SNR Liquid-Phase TEM Videos

The need for unbiased, robust, and automated analysis and interpretation of liquid-phase TEM videos invites new data-mining techniques. Due to the existence of solvent along the electron beam path, the contrast of the features of interest in liquid-phase TEM can be much lower compared to that in dried TEM. In addition, noise in the background increases with decreased electron dose rates following the Poisson distribution,[46] although usage of low-dose rates in liquid-phase TEM has become standard to minimize electron beam effects.

https://dx.doi.org/10.1021/accountsmr.0c00013
Acc. Mater. Res. XXXX, XXX, XXX−XXX

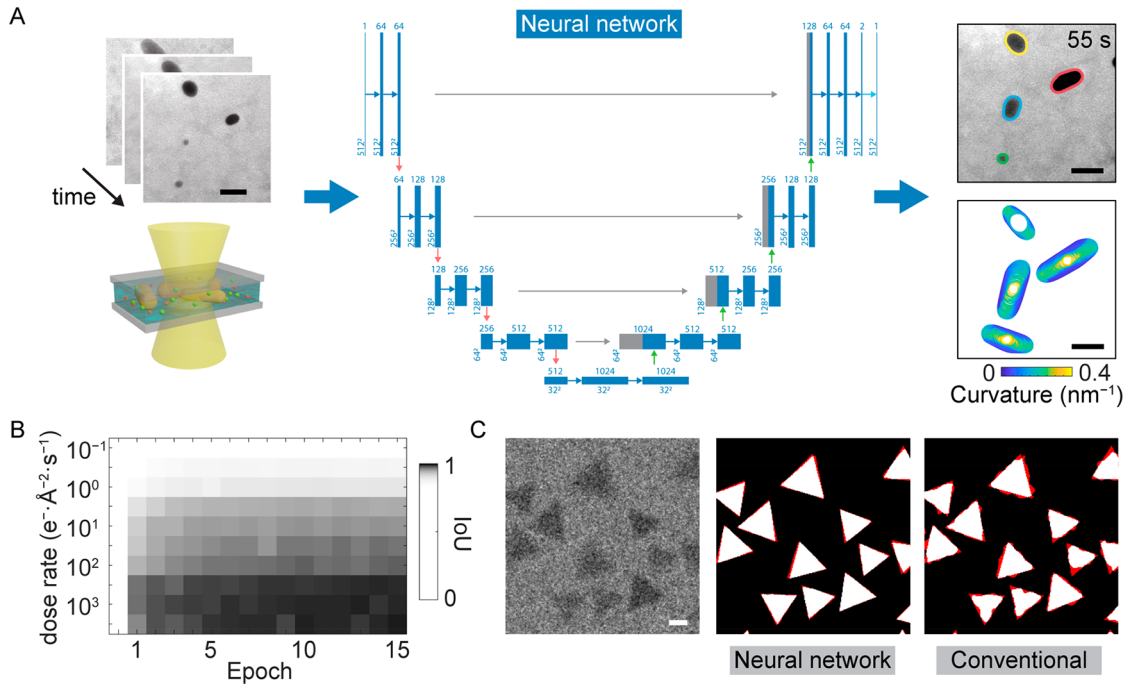

Figure 8. Machine learning for low SNR liquid-phase TEM videos. (A) Workflow of segmentation for time-lapse TEM images through U-Net neural network. (B) Plot of intersection-over-union (IoU) during training over number of epochs and dose rates. (C) Simulated liquid-phase TEM image (left), with comparison of segmentation results between neural network (middle) and conventional method (right). Red regions indicate the deviation of the prediction from ground truth. Scale bars = 50 nm. Reproduced with permission from ref 43. Copyright 2020 American Chemical Society.

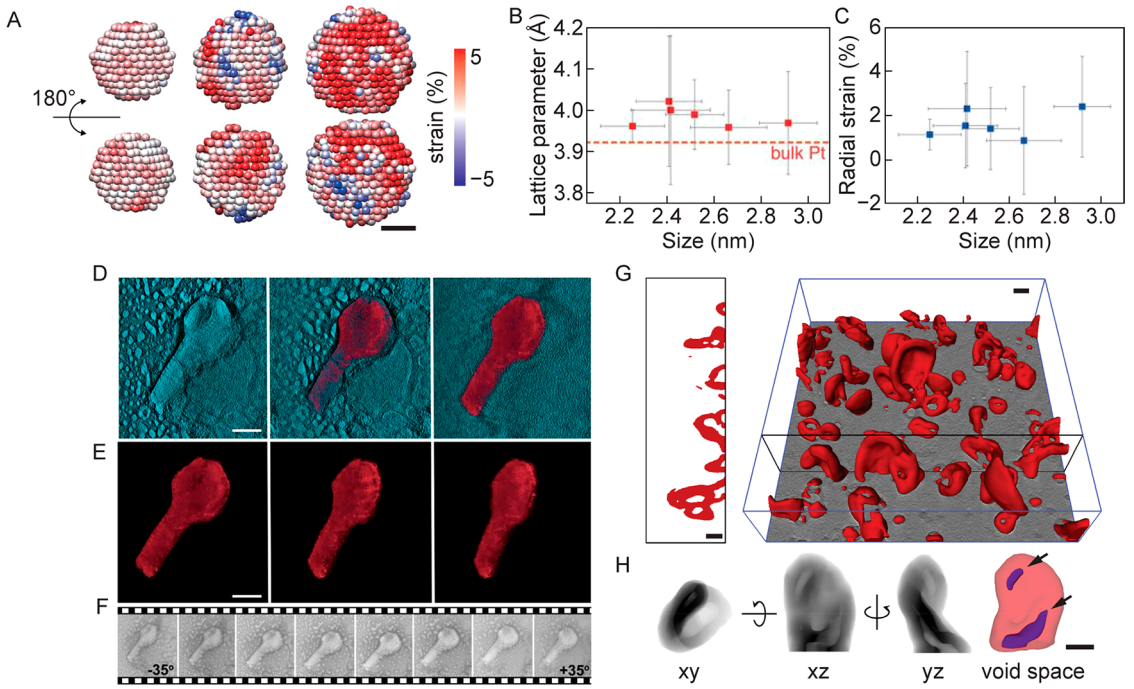

Figure 9. Electron tomography for nanoscale matter. (A–C) Radial strain maps (A), fitted lattice parameters (B), and averaged radial strain values (C) of single-crystalline Pt particles. Scale bar = 1 nm. (D–F) Segmentation of a bacteriophage. (D) Image series and (E) density maps showing the segmentation of a bacteriophage (magenta) from the liquid background (cyan). Scale bars = 50 nm. (F) Tilt images of a phage particle. (G) 2D slice and 3D view of the polyamide membrane after reconstruction. (H) Individual crumples segmented from the 3D data set resolving various projections and interior void (purple). Scale bars = 50 nm. Panels A–C reproduced with permission from ref 47. Copyright 2020 AAAS. Panels D–F reproduced with permission from ref 48. Copyright 2019 American Chemical Society. Panels G and H reproduced with permission from ref 49. Copyright 2019 American Chemical Society.

The "low SNR" challenge in translating liquid-phase TEM videos to digitalized information only worsens when the generic TEM contrast of organic soft matter is low. Thresholding or other algorithms like set evolution and

https://dx.doi.org/10.1021/accountsmr.0c00013
Acc. Mater. Res. XXXX, XXX, XXX−XXX

intelligent scissors need parameter optimization or human supervision, compromising the high-throughput advantage of computerized data analysis.

In our recent effort to introduce the most recent data-mining development of machine learning to liquid-phase TEM videos, we customize a neural network workflow to accurately segment sample features from a noisy background with minimal human input (Figure 8A),[43] as one of the most important tasks of image processing. Using a U-Net convolutional neural network architecture, nanosized entities imaged by liquid-phase TEM at dose rates as low as 1 e^{-} $Å^{-2}$ s^{-1} (typically used for imaging organic soft matter) are successfully segmented from the low SNR images (Figure 8B). The training data set is generated following our protocol of simulating liquid-phase TEM images by considering all the noises in experiment and their spatial correlation (protocol available online).[43] While this protocol has been demonstrated only for metal nanoparticles, its foundation on the general image-forming principles of TEM applies to organic soft matter by considering additional phase contrast.[46]

The trained neural network can process hundreds of experimental liquid-phase TEM images within minutes.[43] Quantitative comparison with traditional segmentation shows a consistently higher precision of machine learning method for liquid-phase TEM images (Figure 8C). The complicated architecture of the neural network can mimic the decision-making process of human brains, which weighs many factors such as local intensity, spatial correlation, and "trained" expectation based on previous experiences to give more accurate predictions. Beyond this first proof-of-concept, we envision application of more advanced machine learning methods in liquid-phase TEM studies such as multiple class image segmentation to differentiate phases or species and instance segmentation to individually detect every nanoparticle.

4.2. Electron Tomography and Cellular Morphometry of 3D Shapes of Organic Soft Matter

Regarding elucidating the 3D shapes of nanosized entities, electron tomography works by capturing a series of TEM images of the same sample region at different tilt angles. In its frontier of imaging 3D shapes in liquids, Park and co-workers have developed the method of structure identification of nanoparticles by graphene liquid cell electron microscopy (SINGLE), where the 3D atomic level structure and strain of Pt nanoparticles can be reconstructed from rotational trajectories given that enough 2D projected views of the same nanoparticle in different orientations are collected (Figure 9A−C).[47] Although hitherto used for inorganic nanoparticles imaged at high dose rates, SINGLE in principle is compatible with organic soft matter to achieve reconstruction of 3D morphologies in liquids at nanometer resolution. Meanwhile, Kelly and co-workers have demonstrated the first liquid-cell electron tomography study where tilt series of a phage capsid was collected to reconstruct its 3D structure (Figure 9D−F).[48] In comparison to SINGLE, this protocol is currently limited to the relatively low tilt angle range due to the use of SiN_x chips of a limited window size (up to ±45° in this work[48]), which could cause the missing wedge effect. Integration of liquid cell electron tomography with a graphene sandwich could potentially allow for a wider range of tilt angles and reconstruction of more complex shapes. Meanwhile, the tilt series in electron tomography are associated with known tilt angles, which can be advantageous over SINGLE where the orientation of each projected view could only be inferred from iterative reconstruction. Complementary to these two seminal works of resolving 3D shapes in liquids, we adapted low-dose electron tomography to the more complex shaped organic matter of a polyamide membrane, which is amorphous, irregular, and spatially heterogeneous with inner structures, all of which we image for the first time (Figure 9G,H).[49] To minimize the beam damage, the tilt TEM image series are taken at a low dose rate of 7.4 e^{-} $Å^{-2}$ s^{-1}. Successful reconstruction is realized at a voxel resolution of 6.8 Å, which reveals nanoscopic crumples with inner voids that are inaccessible by other means, such as surface area and interconnectivity of single crumples. Quantitative analysis of local surface curvature groups the seemingly unrelated polyamide crumples into three distinct classes, which influence the performance of the filtration membrane by changing the affinity and diffusion length of ions inside the membranes.

Apart from the techniques mentioned above, complete 3D morphology of dynamic soft matter in liquids can be potentially resolved with other recent advancements in electron microscopy such as ultrafast electron tomography, focus-based 3D imaging with *z*-slices, and fast cameras to capture not only a 3D shape but its temporal evolution.

5. OUTLOOK

We have discussed our efforts to advance liquid-phase TEM based nanoscopic cinematography as a standard tool to characterize soft matter in its native liquid environment at nanometer resolution. Beyond charting kinetic pathways of self-organization and measuring energetic parameters for computer-designed materials, our vision of using cinematography is 3-fold. First is to enable "in-situ modulation while monitoring or reconfiguring", essential to encode not only self-organization but self-reorganization in nanomaterials to achieve responsive, time-varying functions, such as active plasmonics and metamaterials.[4,6] Second is to provoke crosstalk among traditionally disparate disciplines. One can envision, in the example of atomic-mimicry, building connections in disciplines focused on different sized constituents, such as mineralogy, semiconductor engineering, and colloidal physics.[2,9] Third is to push the boundaries for organic soft matter where a myriad of systems with contemporary significances reside, such as the degradation of polymers into nanoplastics, which have raised concerns for our ecosystem.[50] As to imaging biomolecules, molecular dynamics simulations can provide atomic coordinates of proteins for simulating liquid-phase TEM images, to back out protein structures at atomic resolution through iteration.[46] This effort can shift the paradigm of morphology informed structure elucidation to function mapping.

AUTHOR INFORMATION

Corresponding Author

Qian Chen − *Department of Materials Science and Engineering, Materials Research Laboratory, Beckman Institute for Advanced Science and Technology, and Department of Chemistry, University of Illinois at Urbana−Champaign, Urbana, Illinois 61801, United States;* orcid.org/0000-0002-1968-441X; Email: qchen20@illinois.edu

https://dx.doi.org/10.1021/accountsmr.0c00013
Acc. Mater. Res. XXXX, XXX, XXX−XXX

Authors

Zihao Ou − *Department of Materials Science and Engineering, University of Illinois at Urbana−Champaign, Urbana, Illinois 61801, United States;* orcid.org/0000-0003-2987-7423

Chang Liu − *Department of Materials Science and Engineering, University of Illinois at Urbana−Champaign, Urbana, Illinois 61801, United States;* orcid.org/0000-0001-8091-7940

Lehan Yao − *Department of Materials Science and Engineering, University of Illinois at Urbana−Champaign, Urbana, Illinois 61801, United States;* orcid.org/0000-0003-1945-833X

Complete contact information is available at: https://pubs.acs.org/10.1021/accountsmr.0c00013

Author Contributions

The manuscript was written through contributions of all authors.

Notes

The authors declare no competing financial interest.

Biographies

Zihao Ou obtained his B.S. in Physics from University of Science and Technology of China (2015) and his Ph.D. from University of Illinois at Urbana−Champaign (UIUC) in Professor Qian Chen's group in Materials Science and Engineering in 2020. He is interested in exploring phase behaviors of nanomaterials.

Chang Liu obtained his B.S. in Physics from Nanjing University (2017). He is currently a Ph.D. candidate in Professor Qian Chen's group at UIUC. He is interested in exploring soft matter physics and materials properties and design with liquid-phase TEM.

Lehan Yao obtained his B.S. in Materials Science and Engineering from Soochow University (2018). He is currently a Ph.D. precandidate in Professor Qian Chen's group at UIUC. He is interested in developing machine learning for liquid-phase TEM and patchy nanoparticle synthesis and self-assembly.

Qian Chen obtained her Ph.D. in Materials Science and Engineering at UIUC (2012) and is currently an assistant professor in the same department. She is interested in studying the structure, form, and function of soft matter at the nanoscale.

■ ACKNOWLEDGMENTS

This work was supported by the National Science Foundation under Grant No. 1752517.

■ REFERENCES

(1) de Gennes, P.-G. Soft Matter (Nobel Lecture). *Angew. Chem., Int. Ed. Engl.* **1992**, *31*, 842−845.
(2) Li, B.; Zhou, D.; Han, Y. Assembly and Phase Transitions of Colloidal Crystals. *Nat. Rev. Mater.* **2016**, *1*, 15011.
(3) von Diezmann, A.; Shechtman, Y.; Moerner, W. E. Three-Dimensional Localization of Single Molecules for Super-Resolution Imaging and Single-Particle Tracking. *Chem. Rev.* **2017**, *117*, 7244−7275.
(4) Ou, Z.; Kim, A.; Huang, W.; Braun, P. V.; Li, X.; Chen, Q. Reconfigurable Nanoscale Soft Materials. *Curr. Opin. Solid State Mater. Sci.* **2019**, *23*, 41−49.
(5) Ross, F. M. Opportunities and Challenges in Liquid Cell Electron Microscopy. *Science* **2015**, *350*, aaa9886.
(6) Boles, M. A.; Engel, M.; Talapin, D. V. Self-Assembly of Colloidal Nanocrystals: From Intricate Structures to Functional Materials. *Chem. Rev.* **2016**, *116*, 11220−11289.
(7) Sadeghi, O.; Amiri, M.; Reinheimer, E. W.; Nyman, M. The Role of Bi^{3+} in Promoting and Stabilizing Iron Oxo Clusters in Strong Acid. *Angew. Chem., Int. Ed.* **2018**, *57*, 6247−6250.
(8) Mass, T.; Giuffre, A. J.; Sun, C.-Y.; Stifler, C. A.; Frazier, M. J.; Neder, M.; Tamura, N.; Stan, C. V.; Marcus, M. A.; Gilbert, P. U. P. A. Amorphous Calcium Carbonate Particles Form Coral Skeletons. *Proc. Natl. Acad. Sci. U. S. A.* **2017**, *114*, E7670−E7678.
(9) De Yoreo, J. J.; Gilbert, P. U.; Sommerdijk, N. A.; Penn, R. L.; Whitelam, S.; Joester, D.; Zhang, H.; Rimer, J. D.; Navrotsky, A.; Banfield, J. F.; Wallace, A. F.; Michel, F. M.; Meldrum, F. C.; Colfen, H.; Dove, P. M. Crystallization by Particle Attachment in Synthetic, Biogenic, and Geologic Environments. *Science* **2015**, *349*, aaa6760.
(10) Silvera Batista, C. A.; Larson, R. G.; Kotov, N. A. Nonadditivity of Nanoparticle Interactions. *Science* **2015**, *350*, 1242477.
(11) Kim, B. H.; Yang, J.; Lee, D.; Choi, B. K.; Hyeon, T.; Park, J. Liquid-Phase Transmission Electron Microscopy for Studying Colloidal Inorganic Nanoparticles. *Adv. Mater.* **2018**, *30*, 1703316.
(12) Wu, H.; Friedrich, H.; Patterson, J. P.; Sommerdijk, N. A. J. M.; Jonge, N. Liquid-Phase Electron Microscopy for Soft Matter Science and Biology. *Adv. Mater.* **2020**, *32*, 2001582.
(13) Smith, J. W.; Chen, Q. Liquid-Phase Electron Microscopy Imaging of Cellular and Biomolecular Systems. *J. Mater. Chem. B* **2020**, *8*, 8490−8506.
(14) Luo, B.; Smith, J. W.; Ou, Z.; Chen, Q. Quantifying the Self-Assembly Behavior of Anisotropic Nanoparticles Using Liquid-Phase Transmission Electron Microscopy. *Acc. Chem. Res.* **2017**, *50*, 1125−1133.
(15) Kim, J.; Jones, M. R.; Ou, Z.; Chen, Q. In Situ Electron Microscopy Imaging and Quantitative Structural Modulation of Nanoparticle Superlattices. *ACS Nano* **2016**, *10*, 9801−9808.
(16) Kim, J.; Ou, Z.; Jones, M. R.; Song, X.; Chen, Q. Imaging the Polymerization of Multivalent Nanoparticles in Solution. *Nat. Commun.* **2017**, *8*, 761.
(17) Ou, Z.; Wang, Z.; Luo, B.; Luijten, E.; Chen, Q. Kinetic Pathways of Crystallization at the Nanoscale. *Nat. Mater.* **2020**, *19*, 450−455.
(18) Ou, Z.; Yao, L.; An, H.; Shen, B.; Chen, Q. Imaging How Thermal Capillary Waves and Anisotropic Interfacial Stiffness Shape Nanoparticle Supracrystals. *Nat. Commun.* **2020**, *11*, 4555.
(19) Cameron Varano, A.; Rahimi, A.; Dukes, M. J.; Poelzing, S.; McDonald, S. M.; Kelly, D. F. Visualizing Virus Particle Mobility in Liquid at the Nanoscale. *Chem. Commun.* **2015**, *51*, 16176−16179.
(20) Pohlmann, E. S.; Patel, K.; Guo, S.; Dukes, M. J.; Sheng, Z.; Kelly, D. F. Real-Time Visualization of Nanoparticles Interacting with Glioblastoma Stem Cells. *Nano Lett.* **2015**, *15*, 2329−2335.
(21) Moser, T. H.; Mehta, H.; Park, C.; Kelly, R. T.; Shokuhfar, T.; Evans, J. E. The Role of Electron Irradiation History in Liquid Cell Transmission Electron Microscopy. *Sci. Adv.* **2018**, *4*, eaaq1202.
(22) Keskin, S.; Besztejan, S.; Kassier, G.; Manz, S.; Bücker, R.; Riekeberg, S.; Trieu, H. K.; Rentmeister, A.; Miller, R. J. D. Visualization of Multimerization and Self-Assembly of DNA-Functionalized Gold Nanoparticles Using In-Liquid Transmission Electron Microscopy. *J. Phys. Chem. Lett.* **2015**, *6*, 4487−4492.
(23) Brintlinger, T.; Love, C.; Baturina, O. Beam Effects During In Situ Potential Cycling and Imaging of Sulfuric Acid and Platinum Electrodes. *Microsc. Microanal.* **2015**, *21*, 1935−1936.
(24) Tan, S. F.; Anand, U.; Mirsaidov, U. Interactions and Attachment Pathways between Functionalized Gold Nanorods. *ACS Nano* **2017**, *11*, 1633−1640.
(25) Tan, S. F.; Raj, S.; Bisht, G.; Annadata, H. V.; Nijhuis, C. A.; Král, P.; Mirsaidov, U. Nanoparticle Interactions Guided by Shape-Dependent Hydrophobic Forces. *Adv. Mater.* **2018**, *30*, 1707077.
(26) Tian, X.; Zheng, H.; Mirsaidov, U. Aggregation Dynamics of Nanoparticles at Solid−Liquid Interfaces. *Nanoscale* **2017**, *9*, 10044−10050.
(27) Lee, J.; Nakouzi, E.; Song, M.; Wang, B.; Chun, J.; Li, D. Mechanistic Understanding of the Growth Kinetics and Dynamics of Nanoparticle Superlattices by Coupling Interparticle Forces from Real-Time Measurements. *ACS Nano* **2018**, *12*, 12778−12787.

https://dx.doi.org/10.1021/accountsmr.0c00013
Acc. Mater. Res. XXXX, XXX, XXX−XXX

(28) Park, J. H.; Schneider, N. M.; Grogan, J. M.; Reuter, M. C.; Bau, H. H.; Kodambaka, S.; Ross, F. M. Control of Electron Beam-Induced Au Nanocrystal Growth Kinetics through Solution Chemistry. *Nano Lett.* **2015**, *15*, 5314−5320.
(29) Robertson, A. W.; Zhu, G.; Mehdi, B. L.; Jacobs, R. M. J.; De Yoreo, J.; Browning, N. D. Nanoparticle Immobilization for Controllable Experiments in Liquid-Cell Transmission Electron Microscopy. *ACS Appl. Mater. Interfaces* **2018**, *10*, 22801−22808.
(30) Ahn, T.-Y.; Hong, S.-P.; Kim, S.-I.; Kim, Y.-W. In Situ Liquid-Cell Transmission Electron Microscopy for Direct Observation of Concentration-Dependent Growth and Dissolution of Silver Nanoparticles. *RSC Adv.* **2015**, *5*, 82342−82345.
(31) Wu, J.; Gao, W.; Wen, J.; Miller, D. J.; Lu, P.; Zuo, J.-M.; Yang, H. Growth of Au on Pt Icosahedral Nanoparticles Revealed by Low-Dose In Situ TEM. *Nano Lett.* **2015**, *15*, 2711−2715.
(32) Lin, G.; Chee, S. W.; Raj, S.; Král, P.; Mirsaidov, U. Linker-Mediated Self-Assembly Dynamics of Charged Nanoparticles. *ACS Nano* **2016**, *10*, 7443−7450.
(33) Niu, K.-Y.; Liao, H.-G.; Zheng, H. Visualization of the Coalescence of Bismuth Nanoparticles. *Microsc. Microanal.* **2014**, *20*, 416−424.
(34) Niu, K.; Frolov, T.; Xin, H. L.; Wang, J.; Asta, M.; Zheng, H. Bubble Nucleation and Migration in a Lead−Iron Hydr(Oxide) Core−Shell Nanoparticle. *Proc. Natl. Acad. Sci. U. S. A.* **2015**, *112*, 12928−12932.
(35) Lin, G.; Zhu, X.; Anand, U.; Liu, Q.; Lu, J.; Aabdin, Z.; Su, H.; Mirsaidov, U. Nanodroplet-Mediated Assembly of Platinum Nanoparticle Rings in Solution. *Nano Lett.* **2016**, *16*, 1092−1096.
(36) Jin, B.; Sushko, M. L.; Liu, Z.; Jin, C.; Tang, R. In Situ Liquid Cell TEM Reveals Bridge-Induced Contact and Fusion of Au Nanocrystals in Aqueous Solution. *Nano Lett.* **2018**, *18*, 6551−6556.
(37) Zheng, H.; Smith, R. K.; Jun, Y.-w.; Kisielowski, C.; Dahmen, U.; Alivisatos, A. P. Observation of Single Colloidal Platinum Nanocrystal Growth Trajectories. *Science* **2009**, *324*, 1309−1312.
(38) Lu, J.; Aabdin, Z.; Anand, U.; Mirsaidov, U. Effect of Electron Beam on Nanoparticle Dynamics in Solution during in situ TEM Observation. *Microsc. Microanal.* **2015**, *21*, 257−258.
(39) Chen, Y.-C.; Chen, J.-Y.; Wu, W.-W. In Situ Observation of Au Nanostructure Evolution in Liquid Cell TEM. *J. Phys. Chem. C* **2017**, *121*, 26069−26075.
(40) Aabdin, Z.; Lu, J.; Zhu, X.; Anand, U.; Loh, N. D.; Su, H.; Mirsaidov, U. Bonding Pathways of Gold Nanocrystals in Solution. *Nano Lett.* **2014**, *14*, 6639−6643.
(41) Wang, M.; Dissanayake, T. U.; Park, C.; Gaskell, K.; Woehl, T. J. Nanoscale Mapping of Nonuniform Heterogeneous Nucleation Kinetics Mediated by Surface Chemistry. *J. Am. Chem. Soc.* **2019**, *141*, 13516−13524.
(42) Liu, C.; Ou, Z.; Guo, F.; Luo, B.; Chen, W.; Qi, L.; Chen, Q. "Colloid−Atom Duality" in the Assembly Dynamics of Concave Gold Nanoarrows. *J. Am. Chem. Soc.* **2020**, *142*, 11669−11673.
(43) Yao, L.; Ou, Z.; Luo, B.; Xu, C.; Chen, Q. Machine Learning to Reveal Nanoparticle Dynamics from Liquid-Phase TEM Videos. *ACS Cent. Sci.* **2020**, *6*, 1421−1430.
(44) Chen, Q.; Cho, H.; Manthiram, K.; Yoshida, M.; Ye, X.; Alivisatos, A. P. Interaction Potentials of Anisotropic Nanocrystals From the Trajectory Sampling of Particle Motion Using in Situ Liquid Phase Transmission Electron Microscopy. *ACS Cent. Sci.* **2015**, *1*, 33−39.
(45) Anand, U.; Lu, J.; Loh, D.; Aabdin, Z.; Mirsaidov, U. Hydration Layer-Mediated Pairwise Interaction of Nanoparticles. *Nano Lett.* **2016**, *16*, 786−790.
(46) Rullgård, H.; Öfverstedt, L. G.; Masich, S.; Daneholt, B.; Öktem, O. Simulation of Transmission Electron Microscope Images of Biological Specimens. *J. Microsc.* **2011**, *243*, 234−256.
(47) Kim, B. H.; Heo, J.; Kim, S.; Reboul, C. F.; Chun, H.; Kang, D.; Bae, H.; Hyun, H.; Lim, J.; Lee, H.; Han, B.; Hyeon, T.; Alivisatos, A. P.; Ercius, P.; Elmlund, H.; Park, J. Critical Differences in 3D Atomic Structure of Individual Ligand-Protected Nanocrystals in Solution. *Science* **2020**, *368*, 60−67.
(48) Dearnaley, W. J.; Schleupner, B.; Varano, A. C.; Alden, N. A.; Gonzalez, F.; Casasanta, M. A.; Scharf, B. E.; Dukes, M. J.; Kelly, D. F. Liquid-Cell Electron Tomography of Biological Systems. *Nano Lett.* **2019**, *19*, 6734−6741.
(49) Song, X.; Smith, J. W.; Kim, J.; Zaluzec, N. J.; Chen, W.; An, H.; Dennison, J. M.; Cahill, D. G.; Kulzick, M. A.; Chen, Q. Unraveling the Morphology−Function Relationships of Polyamide Membranes Using Quantitative Electron Tomography. *ACS Appl. Mater. Interfaces* **2019**, *11*, 8517−8526.
(50) Koelmans, A. A.; Mohamed Nor, N. H.; Hermsen, E.; Kooi, M.; Mintenig, S. M.; De France, J. Microplastics in Freshwaters and Drinking Water: Critical Review and Assessment of Data Quality. *Water Res.* **2019**, *155*, 410−422.

https://dx.doi.org/10.1021/accountsmr.0c00013
Acc. Mater. Res. XXXX, XXX, XXX−XXX